GT2013-94328

SENSITIVITY OF THE NUMERICAL PREDICTION OF FLOW IN THE LIMOUSINE COMBUSTOR ON THE CHOSEN MESH AND TURBULENT COMBUSTION MODEL

Mina Shahi[1]   **Jim.B.W.Kok[1]**   **Artur.K.Pozarlik[1]**

J.C. Roman Casado[1]   **Thomas Sponfeldner[2]**

[1] University of Twente, Faculty of Engineering Technology, Laboratory of Thermal Engineering
Enschede, The Netherlands
Email: m.shahi@utwente.nl
[2] Department of Mechanical Engineering, Imperial College London, London, UK

ABSTRACT
The objective of this study is to investigate the sensitivity and accuracy of the combustible flow field prediction for the LIMOUSINE combustor with regards to choices in computational mesh and turbulent combustion model. The LIMOUSINE combustor is a partially premixed bluff body stabilized natural gas combustor designed to operate at 40-80 kW and atmospheric pressure and used to study combustion instabilities. The transient simulation of a turbulent combusting flow with the purpose to study thermo-acoustic instabilities is a very time consuming process. For that reason the meshing approach leading to accurate numerical prediction, known sensitivity, and reduced amount of mesh elements is important. Since the numerical dissipation (and dispersion) is highly dependent on, and affected by, the geometrical mesh quality, it is of high importance to control the mesh distribution and element size across the numerical model. Typically, the structural mesh topology allows using much less grid elements compared to the unstructured grid, however an unstructured mesh is favorable for flows in complex geometries. To explore computational stability and accuracy, the numerical dissipation of the cold flow with mixing of fuel and air is studied first in the absence of the combustion process. Thereafter the studies are extended to combustible flows using standard available ANSYS-CFX combustion models. To validate the predicted variable fields of the combustor's transient reactive flows, the numerical results for dynamic pressure and temperature variations, resolved under structured and unstructured mesh conditions, are compared with experimental data. The obtained results show minor dependence on the used mesh in the velocity and pressure profiles of the investigated grids under non-reacting conditions. More significant differences are observed in the mixing behavior of air and fuel flows. Here the numerical dissipation of the (unstructured) tetrahedral mesh topology is higher than in the case of the (structured) hexahedral mesh. For that reason, the combusting flow resolved with the use of the hexahedral mesh presents better agreement with experimental data and demands less computational effort. Finally in the paper the performance of the combustion model for reacting flow as a function of mesh configuration is presented, and the main issues of the applied combustion modeling are reviewed.

KEYWORDS: structured mesh, unstructured mesh, RANS solver, partially premixed combustion.

INTRODUCTION.

The first step for the CFD calculation is the generation of a mesh in the domain of interest, on which the governing partial differential transport equations can be discretized. Nowadays, many different element and grid types are available, However the choice highly depends on the problem and the solver capabilities, because every method has advantages and disadvantages. One category of meshes are the structured meshes. A structured mesh is a mesh which uses a uniform element shape. The topology of the cells in a structured mesh is specified for the mesh as a whole, and is not deduced from the nodes. Another type of mesh is the so-called unstructured mesh. Unlike a structured mesh, unstructured grids employ an irregular mesh to cover a volume using geometry mesh entities

like faces, edges and nodes [1, 2]. An overview of unstructured mesh techniques for computational fluid dynamics is given by Mavriplis [3] and Kikuchi[4].

In general, structured grid approaches are often used with implicit formulations [5], while unstructured methods seem to be more conveniently used with the explicit formulations [6]. In general, implicit methods used on structured grids seem to be more stable, accurate and converge faster, at least for a large class of practical test cases [7]. In this specific context, to the best knowledge of the authors there is no literature directly evaluating the impact of using fully structured versus unstructured flow solvers on RANS modeling of combustible flows.

Hansen et al. [8] investigated the performance of unstructured grids for turbulence resolving calculations in the application of flow over a circular cylinder at Reynolds numbers 3,900-140,000. They came to the conclusion, that good comparison with experimental data was obtained with the use of structured grids for the Strouhal number, time-averaged drag, back pressure, and recirculation zone length. For simulations of flows at a Reynolds number of 140,000, the time-averaged coefficient of pressure and drag fell within two separate sets of experiments and closely match a similar set of computations on structured grids using a high order of discretization solver.

Studies done by Hua et al. [9] on the flow near a spur-dike indicate that the precision with unstructured grids is higher than that with structured grids in spite that the CPU time required is slightly more with unstructured grids.

Studies done by Tomita et al. [10] showed the strong influence of mesh type on the flow quantities. However they proved that for both structured and unstructured mesh types, the SST turbulence model presented good prediction compared to experiments, while for simulation with other turbulence models like (RSM) results using the structured mesh were superior.

Hence it can be concluded that on basis of the literature the accuracy of the flow simulation is sometimes, but not always, best with a structured solver and it seems to be dependent on the flow geometry and the quality of the mesh generator.

For this reason our purpose in this study is to explore the performance and limitations of certain structured and unstructured grids to investigate the numerical dissipation of the fuel/air mixture flow specifically for the bluff body flow in the LIMOUSINE combustor. The experimental configuration and computational domain are first introduced in Section 1. Section 2 provides the details about the numerical methods, turbulence and combustion models, meshes and sets of boundary conditions used for CFD calculations. Due to the importance of the mixing as a determinant factor in the combustion modeling, the first part of the result section is devoted to the analysis of the mixture flow in the absence of the combustion process. CFD predictions obtained by using a fully structured and a fully unstructured solver are discussed and compared to experiments. Subsequently in the next section,

studies are extended to flows with combustion using combustion models standard available in ANSYS-CFX.

NOMENCLATURE.

BVM   Burning Velocity Model
EDM   Eddy Dissipation Model
FFT   Fast Fourier Transform
FRC   Finite Rate Chemistry Model
P   pressure
T   Temperature
v   streamwise velocity
Φ   Phase of the signal [radian]
λ   Air excess ratio

COMBUSTOR SETUP DESCRIPTION.

The experiment, which is used as a basis for modeling studies, is performed on a test rig which is shown in **FIGURE 1**. It is located at the University of Twente and 4 other laboratories, within the framework of the European Marie Curie Initial Training Network project "LIMOUSINE" (see Annex A). The set-up is designed to study limit cycles of combustion rate oscillations due to thermo-acoustic instability. The combustor consists of two sequentially coupled rectangular ducts with different widths, with the burner in between the two ducts. The duct upstream of the burner has a 25×150 mm^2 cross section and is 275 mm long, whereas the duct downstream the burner has a cross sectional area enlarged to 50×150 mm^2, to partly compensate the volume expansion due to the combustion. In the transition between the ducts the burner is mounted, that creates a flow recirculation pattern, that stabilizes the flame, by means of a triangular bluff body. In this configuration which is the third design version of the combustor (V3), the total length of the combustor is 1050 mm (see TABLE 1 for dimensions). Therefore the width (150 mm) of the combustor is much larger than the depth (50 mm), but much less than the height, and the system approximates in behavior a two dimensional combustor. Details about dimensions of the model combustor are summarized in TABLE 1. Air as the oxidizer is injected at the upstream end. The flow recirculation that stabilizes the flame is in this case created by a wedge, which is placed at the point where the small duct is attached to the large duct. From the side surfaces of the wedge gaseous fuel is injected through 62 holes. The fuel used here is methane at room temperature. All pieces, except the brass bluff body, are made from heat resistant stainless steel S310. The only cooling of the combustor is by natural convection and radiation at the outside surfaces. The burner can operate at a range of power of 20-80 kW and air factor 0.8-2.

This configuration behaves like a variation of a Rijke tube [11], but with forced inlet air flow and closed acoustic upstream condition.

NUMERICAL METHOD.

The CFD code employed here is Ansys CFX 14.0. It uses an implicit finite volume formulation to construct the discretized equations representing the Reynolds Averaged Navier-Stokes

equations for the fluid flow. The model consists of a compressible solver with a co-located (non-staggered) finite volume method, such that the control volumes are identical for all transport equations [12]. To avoid the decoupling of the pressure field, CFX uses the Rhie-Chow [13] discretization method for the mass terms, as modified by Majumdar [14]. A coupled algebraic multi-grid solver is used to give robust solutions for the governing system of linearized equations representing the differential transport equations in discretized form. For the discretization of the governing equations a high resolution advection scheme spatial method and a second order backward Euler discretization for time accuracy is used. The computational geometry used in the solution process is illustrated in FIGURE 2.
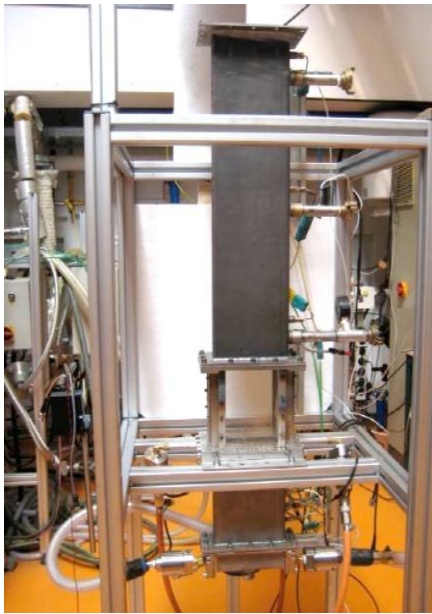
(a)
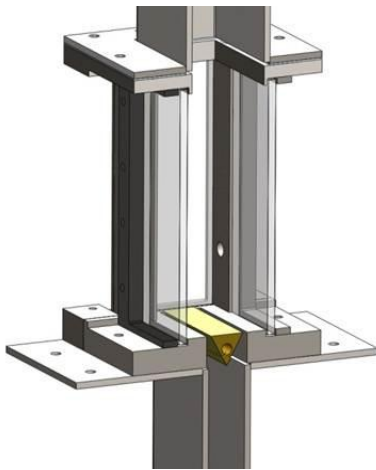
(b)

FIGURE 1 : (A) EXPERIMENTAL SET UP (B) LIMOUSINE BURNER

Details about boundary conditions imposed on the domain are summarized in TABLE 2. The flow parameters are set consistent with the experimental conditions depicted in table 3. The closed acoustic inlet boundary condition at the upstream end was implemented by prescribing a uniform and steady inlet velocity profile at the air inlet, which ensured an acoustically closed inlet. The mass flow rate of fuel per unit cross sectional area was specified at the fuel inlet. A reflecting boundary condition was implemented at the combustor outlet by setting the pressure at that location to a constant value of 1 atm, which represents the open acoustic boundary condition. In order to estimate the effect of heat losses through the walls, the walls were treated as convective boundaries where an outside heat transfer coefficient and outside temperature were specified.

In this work the effects of turbulence are simulated by using the Shear Stress Transport Turbulence Model (SST) in the steady state calculations, while for the transient calculations the Scale-Adaptive Simulation model (SAS) is used. Reacting flow simulations are carried out on the model combustor using different combustion models which are standard available in ANSYS CFX. In the following sections the used turbulence and combustion models are described briefly.

TABLE 1 : DIMENSIONS OF THE MODEL COMBUSTOR.

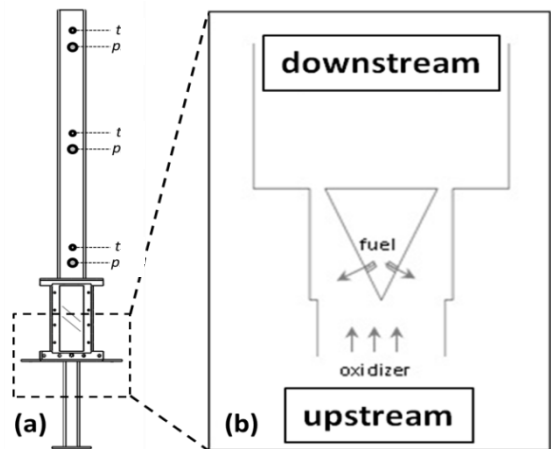| Location	Dimension (mm)
Upstream height	220
Upstream width	25
Downstream height	780
Downstream width	50
Width of the combustor in the third direction	150

FIGURE 2 : A SCHEMATIC REPRESENTATION OF THE MODEL COMBUSTOR: (A) COMPUTATIONAL DOMAIN IN CFD CALCULATION (B) AN ENLARGED VIEW AROUND THE WEDGE.

3   Copyright © 2013 by ASME

TABLE 2: DETAILS ABOUT BOUNDARY CONDITION.

Location	B.C
Air Inlet	Normal speed
Fuel Inlet	Mass flow rate
Outlet	Average static pressure
Walls	Non-slip

TABLE 3: OPERATING CONDITION.

Power (kW)	Air factor	Fuel mass flow rate [gr/s]	Air mass flow rate [gr/s]
40	1.4	0.8	19.152
60	1.2	1.2	24.624

MODELING OF TURBULENCE

THE SST (SHEAR STRESS TRANSPORT) TURBULENCE MODEL

The $k-\varepsilon$ model has two main weakness: over predicting the shear stress in adverse pressure gradient flows, due to too low dissipation, and requirement for wall modification. The $k-\omega$ models model is better in predicting the adverse pressure gradient flow and it does not use any damping functions. However, it is dependent on the value of ω in the free stream flow. In order to improve these models, the SST model suggested by Menter [15] was developed. The SST is an eddy-viscosity model which is using a combination of $k-\varepsilon$ and $k-\omega$ models for the core flow and boundary layer, respectively. For this a blending function F1 is introduced which is equal to one in the near wall region and equal to zero for the flow domain in the outer region. It smoothly switches from the $k-\omega$ model in the near wall region to the $k-\varepsilon$ model for the rest of the flow. In this way, the near-wall performance of the k − ω model can be used without the potential errors resulting from the free stream sensitivity of that model.

The SAS Turbulence Model

The Scale-Adaptive Simulation (SAS) is an advanced URANS model which allows better resolution of the turbulence spectrum in unstable flow conditions. This model can change smoothly between LES-like behavior in regions where the turbulence structure is well resolved and the SST model where the unsteady flow is not well resolved. The starting point of the transformation to the SST model is the k-vt formulation as given by Menter et al.[16].

MODELLING OF THE COMBUSTION

The simulations here have been carried out with the help of four different combustion models (available in ANSYS CFX code), depending on suitability in terms of time and available computer capacity. Their basic principles and features are discussed in Annex B.

RESULTS AND DISCUSSIONS

PART I: MESHING EFFECTS

All the meshes used in this study were generated using the meshing tool ANSYS Workbench 14.0. Since the CFX solver uses the nodes to create control volumes around it, the number of nodes should be chosen as a congruence parameter. The grid which represents the flow domain can be unstructured (composed of hexahedra, tetrahedral, wedges, and pyramid control volume shapes) or structured. In general, structured meshes offer easy data access, while unstructured meshes offer more convenient mesh adaptivity and better fit to complex geometries. The big advantage of using hexa meshes applications is, that one can align the mesh relatively nicely with the flow direction, therefore reducing numerical diffusion and aiding convergence, and less elements are demanded to fill the considered domain at the same time. However it should be noticed that in each approach the mesh adjacent to the wall should be fine enough to resolve the boundary layer flow. In boundary layers, quadrilateral, hexahedron, and prism/wedge cells are preferred over triangles, tetrahedrons, or pyramids.

Considering that all important turbulent structures and stresses are generated close to the wall, it is very important to control the distance of the first element from the wall surface, because different turbulence models have different requirements for mesh treatments to guarantee accurate results. For the unstructured mesh, it is possible to define the smaller and larger element sizes to control this distance from the wall surface. For the structured mesh generation the control of elements distribution near the wall is more robust and the smoothing process as well as the use of different functions are possible. Since the resolution of the grid has significant effects on the accuracy of results, in this work each mesh type was used for three different mesh sizes in each structured and unstructured approach, and the final mesh chosen for simulation is shown in TABLE 4.

FIGURE 3 demonstrates the influence of the number of elements in the present configuration based on the vertical component of velocity profile at three different lines along the length of the combustor for structured and unstructured meshes. These results will be discussed in combination with results on mixing in figure 4..

TABLE 4: NUMBER OF ELEMENTS FOR EACH MESH.

	Structured Mesh	Unstructured Mesh
Number of elements	4,000,822	6,200,000

It can be assumed that in this combustor turbulent diffusion is several orders of magnitude larger than molecular diffusion, and therefore, prediction of turbulent mixing should not be affected by numerical diffusion [17]. FIGURE 4 represents effects of the chosen grid on the mixing behavior. The CH_4 mass concentration obtained by using each grid type is shown in three different cross sectional planes

along the length of the combustor. Much stronger mixing is predicted by the unstructured mesh, probably because of the large amounts of numerical diffusion inherent to these grids (numerical artifact resulting from the use of first order upwind for discretizing convection terms). Indeed in the structured mesh, cells are aligned with the general flow direction giving lower numerical dissipation and lower cell count.

The obtained mixing results in the unstructured grid as well as the velocity profile presented in FIGURE 3 are slightly asymmetric with respect to the center, which is not expected from a physical point of view. Overall, not only these results show how numerical diffusion affects the distribution of species, they also demonstrate how numerical diffusion can cause an unphysical asymmetric velocity profile.

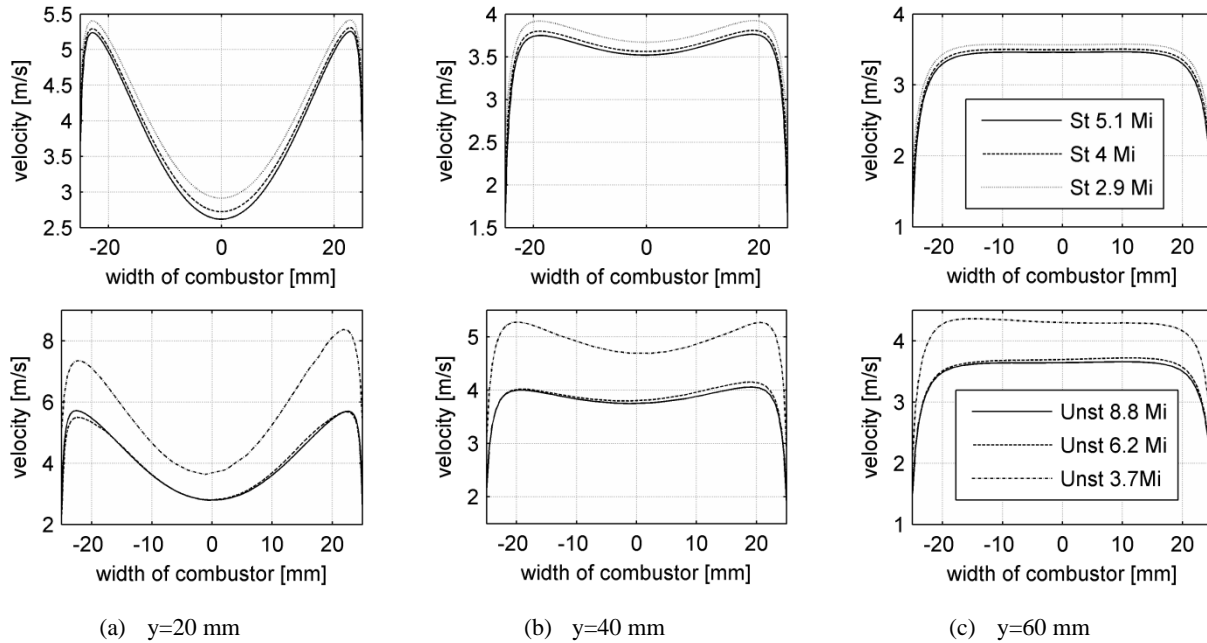(a)   y=20 mm   (b)   y=40 mm   (c)   y=60 mm

FIGURE 3: MESH-DEPENDENCY STUDIES OF STRUCTURED (ST) (ON TOP) AND UNSTRUCTURED MESH (UNST) (ON BOTTOM) BASED ON THE STREAMWISE (vertical component of) VELOCITY.

CH4 mass concentration

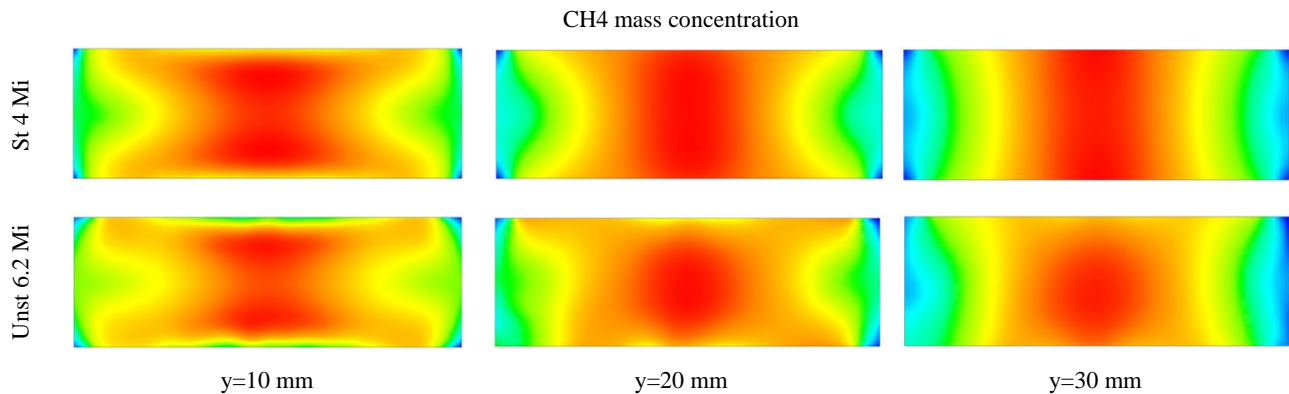y=10 mm   y=20 mm   y=30 mm

FIGURE 4: COMPARISON OF STRUCTURED (ST) AND UNSTRUCTURED MESH (UNST) IN THE MIXING BEHAVIOR.

FIGURE 5 shows a time averaged transient solution of the vertical velocity component, v, in the cold flow simulation, as well as velocity measurements obtained with the Particle Image Velocimetry method (PIV) averaged over 100 images, measured at Imperial College London. In each part of this figure, isocontours of v = 0 are shown which are representing the location of the recirculation zones (labeled in figure 5 with 0). Recirculation occurs in three regions: in the central region (referred as CRZ) which is stabilizing the flame, and also in

two regions between the fresh fuel gas jets and near the liner of the downstream duct referred as (CORZ).

The predictions compare quite well with the measurements in the center and corner recirculation regions, while the velocity magnitude in profiles close to the wall is overpredicted: especially in the case of using the unstructured grid. This can be due to the near-wall treatment used in the simulations and the resulting cell size very close to the wall. A second explanation is that very close to the walls, reflections from the laser beam

tend to under predict the velocity, due to bright spots or deposition of particles etc. And lastly, at downstream positions of around 25 mm the PIV data shows a region of lower velocities. This is due to reflections from the rear window causing under predictions of the velocity similar to the regions close to the side walls. Furthermore the core of the CRZ is more squeezed compared to measured data. However, the

current predictions are able to capture the essential characteristics of the flow (i.e stagnation points etc.). Although there are some differences between simulations and experiments, the predicted pressure fluctuations which will be discussed later show very good agreement with experimental data.
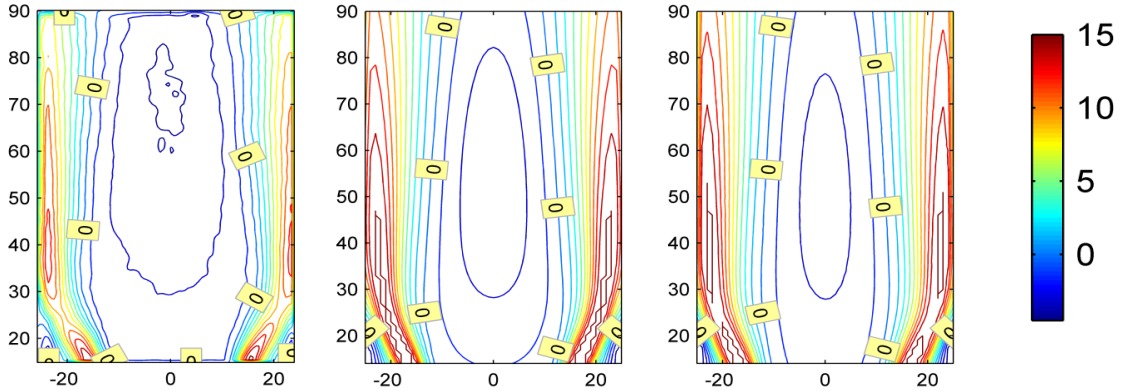
FIGURE 5: STREAM WISE VELOCITY COMPONENT FOR 40 KW THERMAL POWER AND AIR FACTOR 1.4 : EXPERIMENT (LEFT), STRUCTURED MESH (MIDDLE), UNSTRUCTURED MESH (RIGHT).
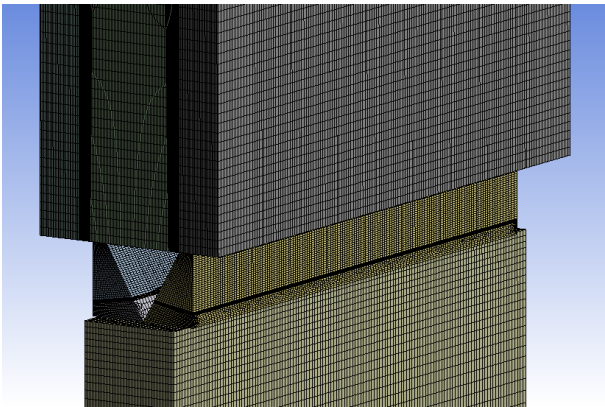

FIGURE 6: DETAILS OF MESH AROUND THE BLUFF BODY FOR THE STRUCTURED MESH
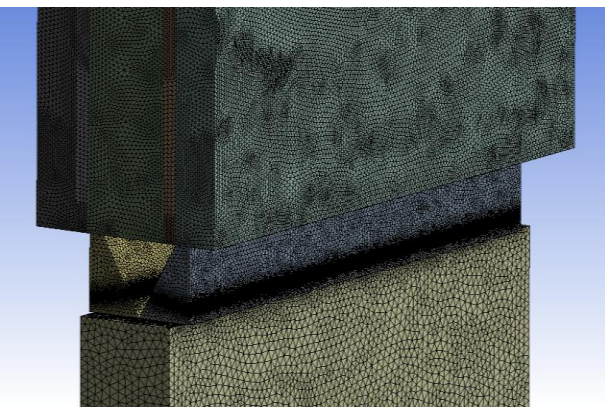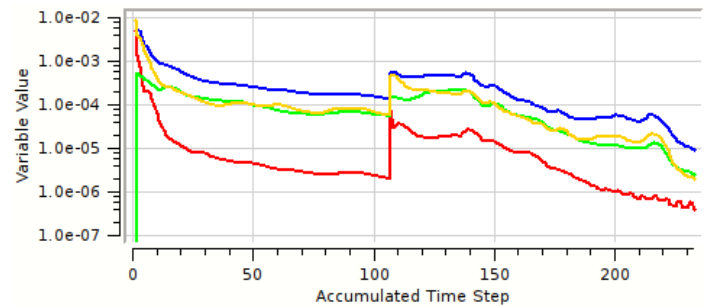

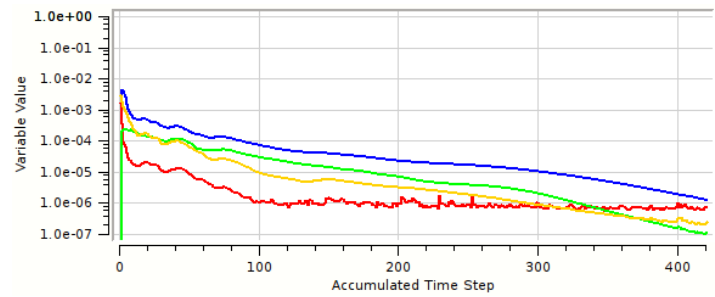FIGURE 7: DETAILS OF MESH AROUND THE BLUFF BODY FOR THE UNSTRUCTURED MESH

FIGURE 8: NUMERICAL RESIDUALS USING STRUCTURED (TOP) AND UNSTRUCTURED MESH (BOTTOM)

FIGURE **6** and FIGURE **7** show the enlarged view of the mesh around the wedge for the structured and unstructured grids, respectively. Due to having very small scales in the geometry (i.e 1mm fuel holes and 3 mm burner passage slots), generating a mesh with good quality and without massive jumps in the element size or introducing high aspect ratios is very difficult. Despite these difficult aspects of the combustor

design, care was taken to keep the aspect ratio, expansion factor and orthogonality angle in the desired range.

FIGURE **8** presents the conserved variables residues history in the simulation process for both mesh methods. It is important to mention that, in the case of the unstructured grid, the numerical procedure started oscillating around residues value of 1e-5. Therefore a dissipative scheme is set up using a first-order discretization for the Navier-Stokes advection terms to avoid numerical instabilities, and then after 100 iterations the discretization order of advection terms in momentum equations was changed back to second order.

PART II: NON-REACTING FLOW

The acoustic phenomenona in a gas turbine combustor can originate from different sources. Vibrating mechanical structures, regions of turbulent flow, mixing of fluids with different temperatures are some examples for sound generation mechanisms. However, earlier performed analysises on different types of noise sources in the combustor chamber, showed that the acoustic noise induced by the unsteady combustion process is the strongest acoustic source [18]. This is of course missing in non-reacting calculations. To determine the exothermic effects on the flow in the model combustor, a non-reacting flow was first simulated as a reference by using different mesh types. The main parameters which were analyzed are: pressure fluctuations, streamwise velocity and also temperature in the case of hot flow. To observe the pressure fluctuations inside the combustion chamber, several locations along the length of the combustor are monitored, which are shown in FIGURE 9. In this figure, P1 to P6 are representing the location of both a CFD monitor points and test rig pressure transducer, while T1 to T4 stand for thermocouple locations.

FIGURE 10 shows the pressure spectra of the isothermal flows in the combustor with **non-reacting** mixture measured and calculated at three pressure transducer locations mounted downstream the bluff body (numbers 4 to 6 in FIGURE 9).
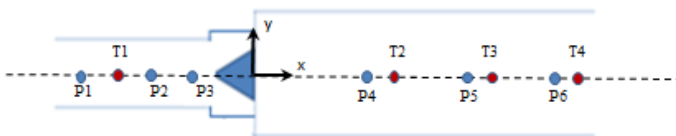

FIGURE 9: PRESSURE AND TEMPERATURE MONITORING POINTS IN THE CFD DOMAIN: UPSTREAM AND DOWNSTREAM OF THE WEDGE.

To have better visualization on the plots, the pressure data obtained from the **unstructured** grid has been **scaled down by a factor 5**. The combustor shows a self-excited acoustic mode at about 90 Hz. Other peaks of lower magnitude can be observed at multiple times the main frequency.

The comparison between the calculated and measured mean velocity on structured and unstructured meshes (FIGURE 5) showed a minor dependence on the used mesh.

The comparison of pressure data shows however an overprediction of a factor of 5 in the amplitude of oscillations by the unstructured mesh simulation in comparison with both measured data and structured mesh simulation data. In addition the first mode calculated using the unstructured grid is under predicted by 20 Hz. The higher harmonics are more damped and not so clear in this scheme.
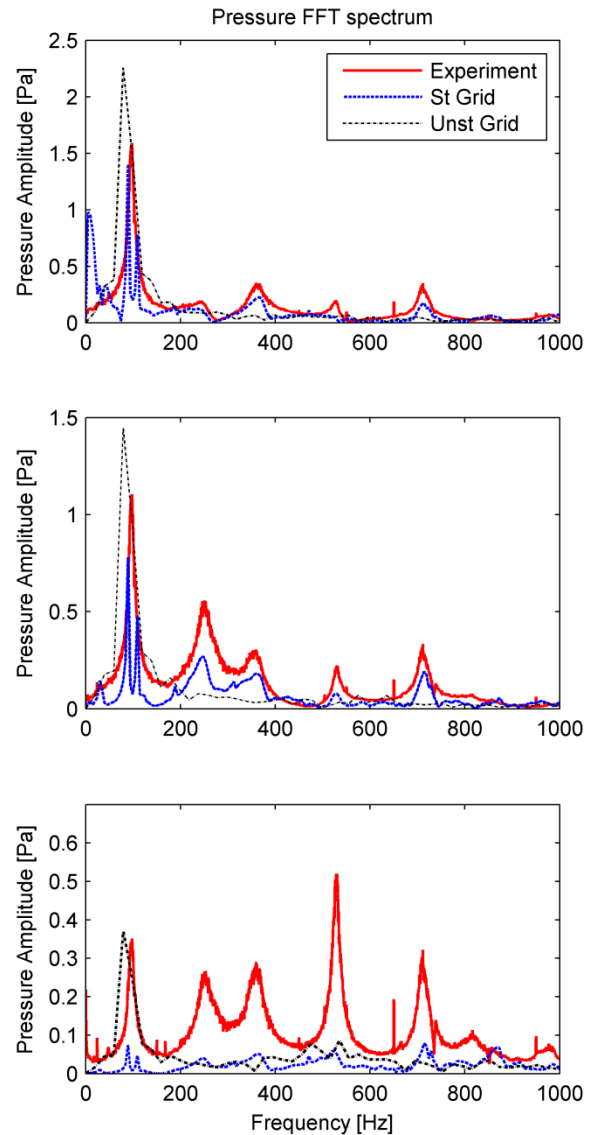

FIGURE 10: FFT FOR 40 KW THERMAL POWER AND AIR FACTOR 1.4: EXPERIMENT, STRUCTURED MESH, UNSTRUCTURED MESH FOR DIFFERENT LOCATIONS. (*UNSTRUCTURED GRID HAS BEEN SCALED DOWN BY A FACTOR 5*).

The multi microphone method (MMM) is applied on the pressure data obtained from the CFD calculations (at the locations of pressure transducers P1 to P6) to reconstruct the acoustic pressure and velocity fields.

FIGURE 11 shows the amplitude of pressure as well as velocity fluctuations, measured at the first and the second peak frequencies against the length of the combustor. The origin of the axial axis in this case is taken at the center of the exit plane. Therefore zero in the x-axis corresponds to the exit of the burner, and the vertical thick line at (-0.78) shows the position of the bluff body.The pressure anti-node at the inlet and the node at the outlet of the combustor confirms that the open-closed acoustic boundary condition is established well by the numerical method. The pressure amplitude decreases along the combustor and the maximum pressure occurs right above the bluff body, which matches the theoretical location of the maximum pressure for the first quarter wave. The pressure profile obtained at the second resonance peak (at about three times the first fundamental frequency) is consistent with the ¾ wavelength resonant mode of an acoustic pipe.
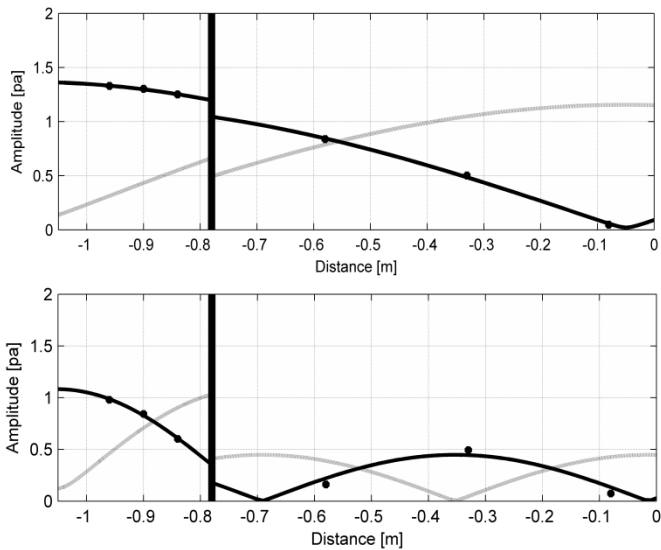

FIGURE 11: PRESSURE (BLACK LINE) AND VELOCITY (GRAY LINE) MODE SHAPE AT THE FIRST FUNDAMENTAL FREQUENCY (TOP) AND AT THE THIRD QUARTER WAVE MODE (BOTTOM) FOR THE STRUCTURED GRID CALCULATIONS.

TABLE 5 represents the values of reflection coefficients at the exit plane, obtained from the simulation based on the structured grid and also from the experiment at the University of Twente for the same operating condition. Quite good agreement can be seen between experiments and CFD data for the values of the reflection coefficients (R). These results prove that the combustor is acoustically open as R tends to unity.

TABLE 5: REFLECTION COEFFICIENTS AND PHASE OF THE SIGNAL CALCULATED AT THE EXIT OF THE COMBUSTOR

CFD		Experiment	
|R|	Φ	|R|	Φ
0.98	-3.00	1	-π

PART III: REACTING FLOW- COMBUSTION MODELING EFFECT

The reacting premixed flow is studied experimentally and also with 4 different combustion models. The reduced GRI MECH 3.0 was chosen as the detailed reference chemical reaction mechanism for these combustion models. This mechanism involves 25 species and 100 reactions for the methane-air gas mixture.

Results are presented in FIGURE **12** for air flow rate 19 g/s and a thermal power of 40 kW. For this flow, three clear self-excited modes are found experimentally at the University of Twente test rig which are around 240 Hz, 480 Hz and 720 Hz. To identify the nature of these modes, a FEM analysis has been done with the average temperature field, given by the experimental data, to obtain the acoustic eigenmodes. As Heckl [19] proposed, due to the area blockage of the burner, it can be assumed that the upstream and the downstream part of the combustor are acoustically decoupled, therefore only the downstream duct has been taken into account in the FEM calculation. The obtained results confirm that the first and the third frequencies observed in the experiment are the first two acoustic modes of the combustor. The measured pressure signal shows limit cycle behavior with strong non-linearities with a peak at twice the fundamental frequency [20]. Besides these modes there are more peaks observed experimentally which correspond to vibrational eigen frequencies of the liner presented in [21]. Pressure fluctuation time history and FFT as obtained from simulations using different combustion models (all available in ANSYS CFX) are presented in FIGURE 12. Failure of the Eddy Dissipation /Finite Rate Chemistry model can be concluded on basis of its prediction of a stable flame (which is not the case for the investigated operating condition).
The PDF Flamelet model in CFX is originally designed for modeling of non-premixed flames. Although testing this model for the LIMOUSINE combustor shows the model is able to predict the instability correctly, it failed in prediction of self-excited modes. The Burning velocity model (BVM) is found to over- predict mean temperature and the rate of conversion to product species. The predicted temperature profiles are consistent with the over-prediction of the molar fraction of major product species.
Fourier analysis of the pressure signal obtained from the BVM model yields two distinct peaks appearing at frequencies of about 319 and 638 Hz. Among the combustion models tested in this paper, that is the only model able to predict the frequency doubling of the first self-excited mode. These peaks were present in the experiment, but with different amplitude and frequencies. Since in this paper the mutual interaction between flow and the vibrating liner (due to the high amplitude thermo-acoustic instabilities) for the numerical computations has been neglected, the effect of the vibrating walls on the combustible flow is only visible in the experimental data. Numerical simulation by using Large Eddy Simulation (LES) at CERFACS in the current combustor also predicted a dominant peak at 305 Hz and also the secondary peak 617Hz, see [22],

which is close to the value calculated by the BVM model. Nevertheless, some discrepancies between numerics and experiment, in the prediction of fundamental frequency in this Bluff body stabilized combustor, the use of the BVM model for other applications on a swirl stabilized flame computations shows promising results compared to the experimental data [23].

CONCLUSION AND FUTURE WORK

In the paper, two structured-unstructured grid techniques in a finite volume method are used to simulate reacting and non-reacting flow in a partially premixed bluff body stabilized model combustor. This paper has presented the performance of the combustion model for reacting configuration, and the main issues of the performed combustion modeling were reviewed. The following conclusions can be drawn from the present study:

- The obtained velocity fields resolved under structured and unstructured mesh conditions show minor dependence on the used mesh in the mean velocity compared to the PIV data, while the pressure fluctuations were found to depend heavily on the investigated grids.
- The unstructured mesh showed larger rates of mixing as compared to the structured mesh and hence this hints at significant numerical diffusion caused by the unstructured mesh discretization.
- Using the Eddy Dissipation/Finite Rate Chemistry combustion model results in an unphysical stable flame (also flash back was observed). Although the PDF Flamelet model is able to predict the instability within the investigated combustion system, it failed in prediction of frequency of the self-excited modes.
- The Burning velocity model (BVM) is found to over-predict the mean temperature and rate of conversion to product species. However this model is able to predict the frequency doubling of the first self-excited mode. To overcome the former problem it is important to improve the boundary condition imposed to the liner . Of significance may be the influence of the prescribed liner boundary condition on the predictions. This influence is likely to be larger than in the stable combustion processes. In order to assess the energy transfer from the combustor to the ambient, beside considering the convection from the liner, heat transfer due to radiation (emission) from the quartz glass windows should be also taken into account.

Our future research targets the improvement of combustion modeling by using the CFI model linked to ANSYS (in-house code developed at University of Twente). The CFI model is a reaction progress variable model coupled to a reduced chemistry database.
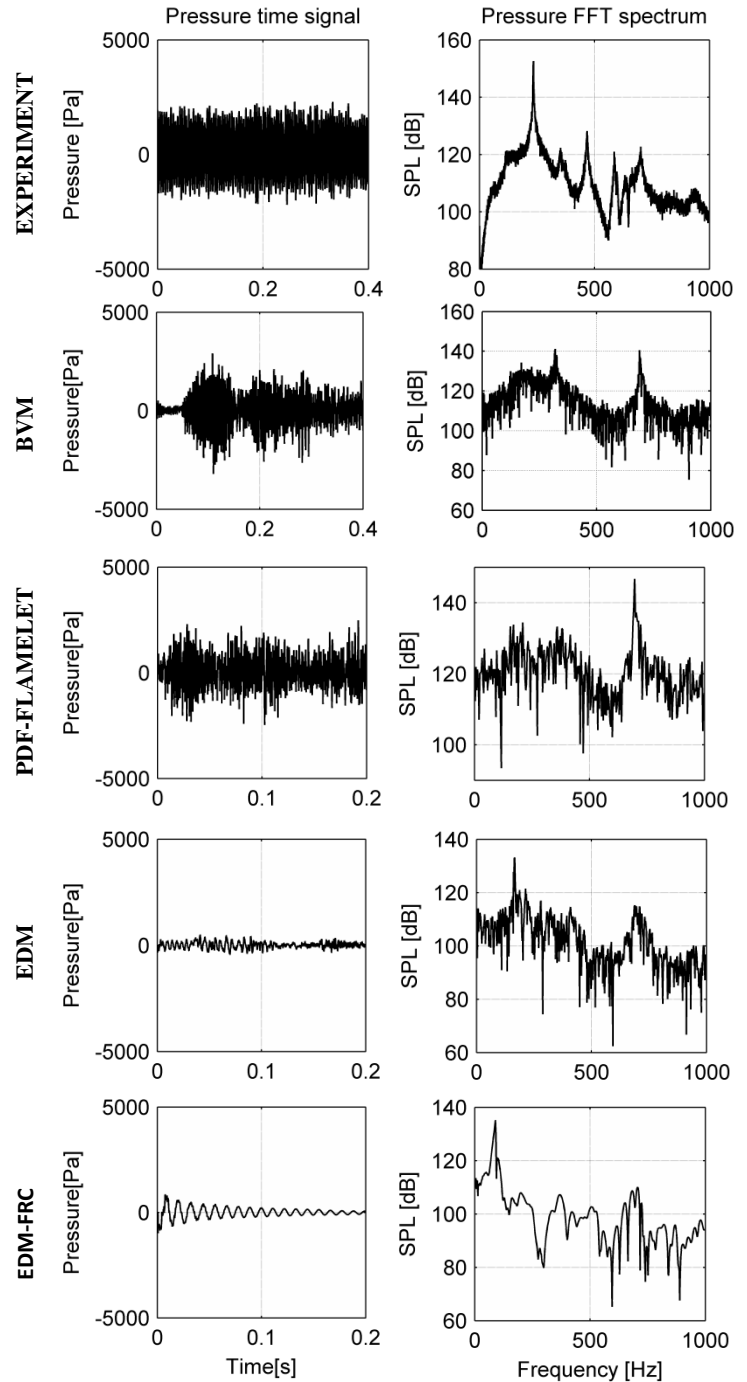

FIGURE 12: PRESSURE FLUCTUATIONS TIME HISTORY AND FFT AT POWER = 40 KW AND Λ=1.4 MEASURED AT A LOCATION 200 MM DOWNSTREAM THE WEDGE

REFERENCES

1. Weatherill, N.P., *A method for generating irregular computational grids in multiply connected planar domains.* International Journal for Numerical Methods in Fluids, 1988. **8**(2): p. 181-197.

2. Koomullil, R., B. Soni, and R. Singh, *A comprehensive generalized mesh system for CFD applications.* Mathematics and Computers in Simulation, 2008. **78**(5–6): p. 605-617.

3. Mavriplis, D.J., *Unstructured grid techniques.* Annual Review of Fluid Mechanics, 1997. **29**: p. 473-514.

4. Kikuchi, N., *Adaptive grid-design methods for finite element analysis.* Computer Methods in Applied Mechanics and Engineering, 1986. **55**(1–2): p. 129-160.

5. Beam RM and R. Warming, *Implicit numerical method for the compressible Navier–Stokes and Euler equations.* Lecture notes of Von Karman institute for fluid dynamics, 1982.

6. Caughey, D.A. and M.M. Hafez, *Frontiers of Computational Fluid Dynamics* 1994, John-Wiley & Sons: New York.

7. Çete, A.R., M.A. Yükselen, and Ü. Kaynak, *A unifying grid approach for solving potential flows applicable to structured and unstructured grid configurations.* Computers & Fluids, 2008. **37**(1): p. 35-50.

8. Hansen, R.P. and J.R. Forsythe, *A Comparison of Structured and Unstructured Grid Solutions for Flow Over a Circular Cylinder*, in *Proceedings of the 2003 DoD User Group Conference* 2003, IEEE Computer Society. p. 104.

9. Hua, Z.-l., L.-h. Xing, and L. Gu, *Application of a modified quick scheme to depth-averaged κ–ε turbulence model based on unstructured grids.* Journal of Hydrodynamics, Ser. B, 2008. **20**(4): p. 514-523.

10. Tomita, J.T., L.M.d. Silva, and D.T.d. Silva. *Comparison between unstructured and structured meshes with different turbulence models for a high pressure turbine application* in *Proceedings of ASME Turbo Expo*. 2012. Copenhagen, Denmark.

11. Rijke, P.L., *On the vibration of the air in a tube open at both ends.* Philosophical Magazine, 1859. **17**: p. 419-422

12. Patankar, S.V., *Numerical Heat Transfer and Fluid Flow* 1980: Hemisphere Publishing Corp.

13. C.M.Rhie and W.L.Chow, *a numerical study of Turbulent Flow Past an Isolated Airfoil with the Trailing Edge Separation.* Aiaa Journal, 1982: p. 82-0998.

14. Majumdar, S., *ROLE OF UNDERRELAXATION IN MOMENTUM INTERPOLATION FOR CALCULATION OF FLOW WITH NONSTAGGERED GRIDS.* Numerical Heat Transfer, 1988. **13**(1): p. 125-132.

15. Menter, F.R., *2-Equation Eddy-Viscosity Turbulence Models for Engineering Applications.* Aiaa Journal, 1994. **32**(8): p. 1598-1605.

16. Menter, F.R. and Y. Egorov, *The Scale-Adaptive Simulation Method for Unsteady Turbulent Flow Predictions. Part 1: Theory and Model Description.* Flow Turbulence and Combustion, 2010. **85**(1): p. 113-138.

17. Liu, M., *Age Distribution in the Kenics Static Micromixer with Convection and Diffusion.* Industrial & Engineering Chemistry Research 2012. **51**(20): p. 7081-7094.

18. Pozarlik, A., *Vibro-Acoustical Instabilities Induced by Combustion Dynamics in Gas Turbine Combustors*, 2010, University of Twente: Enschede, Netherlands.

19. Heckl, M., *the Rijke tube: A green's function approach in the frequency domain.* Acta Acustica united with Acustica, 2010. **96**(4): p. 743-752.

20. J.C.Roman Casado and J.B.W.Kok, *Non-linear effects in a lean partially premixed combustor during limit cycle operation* in *Proceeding of ASME Turbo Expo 2012* 2012: Copenhagen, Denamrk.

21. A. Can Altunlu, et al. *Fluid-structure interaction on the combustion instability*. in *ICSV19*. 2012. Vilnius, Lithuania.

22. Vera, I.H., *Soot modeling in flames and Large-Eddy Simulations of thermo-acoustic instabilities*, 2011, Universite de Toulouse.

23. Ozcan, E., *Tuning the self -excited thermo-acoustic oscilations of a gas turbine combustor to Limit Cycle Operations by means of numerical analysis* in *Faculty of Engineering Thechnology , Labratory of Thermal Engineering* 2012, University of Twente.

24. Rayleigh, J., *The explanation of certain acoustic phenomena.* Nature, 1878. **18**: p. 319-321.

25. Mina Shahi, Jim.B.W.Kok, and P.R.Alemela. *Simulation of 2-way fluid structure interaction in a 3D model combustor*. in *Proceedings of ASME Turbo Expo*. 2012. Copenhagen, Denmark.

26. *ANSYS (2010). Release 11.0 Documentation for ANSYS.*

27. Veynante, D. and L. Vervisch, *Turbulent combustion Modeling.* Prog. in Energy and Comb. Sci, 2002. **28**: p. 193-266.

ANNEX A
LIMIT CYCLES OF THERMO-ACOUSTIC OSCILLATIONS IN GAS TURBINE COMBUSTORS

Limousine is a Marie Curie Initial Training Network funded by the European Commission under Framework 7. It represents a multidisciplinary initiative to strengthen the fundamental scientific work in the field of thermo-acoustic instabilities in combustion systems, and is motivated by the need for lean combustion technologies and reduced emissions. The research in Limousine is focused on the limit cycle behavior of the unstable pressure oscillations in gas turbines, and on the resulting mechanical vibrations and materials fatigue.

Thermo-acoustic instability can be caused by the feedback mechanism between unsteady heat release, acoustic oscillations and flow perturbations. In a gas turbine combustor limit cycles of pressure oscillations at elevated temperatures generated by the unstable combustion process enhance the structural vibration levels of the combustor.

This state-of-the-art generic combustor represents self-exited oscillations of high amplitude. Depending on the operating conditions (thermal power and air/fuel ratio), the flame shows a stable or an unstable behavior. FIGURE **13** shows the stability map of the combustor [21] .

The self-excitation of combustion instabilities is linked to the phase relationship between the acoustic pressure field and unsteady heat release via Rayleigh's criterion[24]. The Rayleigh criterion, which recognizes the difference between damped or amplified interaction between pressure and heat release is often used to investigate and predict combustion instabilities. It states that if pressure and heat release fluctuations are in phase, the instabilities are enhanced, whereas the instabilities are damped when the pressure oscillations and heat release are out of phase. This criterion is expressed as following Equation:

$$\iiint_{\Omega} p'q' \, d\Omega > 0$$

where p' and q' are pressure and heat release fluctuations, respectively, integrated over one cycle of the oscillation and Ω is the flow domain. Note that the integrals are also spatial, which means that both effects, destabilizing and stabilizing, can occur in different locations of the combustor and at different times, so the stability of the combustor will be decided by the net mechanical energy added to the combustor domain. Indeed when the acoustic energy losses match the energy gain stationary oscillatory behavior is obtained which is referred to as the limit cycle oscillation (LCO)[25].
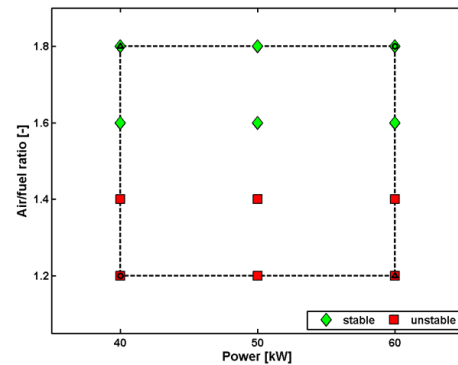
FIGURE 13: STABILITY MAP OF THE LIMOUSINE COMBUSTOR

ANNEX B [26]
MODELLING OF THE COMBUSTION

EDDY DISSIPATION MODEL (EDM

The eddy dissipation model [26] is based on the concept that chemical reaction is fast relative to the transport process in the flow. When reactants mix at the molecular level, they instantaneously form products. The model assumes that the reaction rate may be related directly to the time required to mix reactants at the molecular level.
By default, for the Eddy Dissipation Model it is sufficient that fuel and oxidant be available in the control volume for combustion to occur.

COMBINED EDM/FINITE RATE CHEMISTRY MODEL

For the combined Finite Rate Chemistry/ Eddy Dissipation Model [26], the reaction rates are first computed for each model separately and then the minimum of the two is used. This procedure is applied for each reaction step separately, so while

the rate for one step may be limited by the chemical kinetics, some other step might be limited by turbulent mixing at the same time and physical location.

Use of this model is recommended if reaction rates are limited by turbulent mixing in one area of the domain and limited by kinetics somewhere else.

PDF FLAMELET MODEL

The Flamelet concept [27] for non-premixed combustion, describes the interaction of chemistry with turbulence in the limit of fast reactions (large Damköhler number). The combustion is assumed to occur in thin sheets with inner structure called *Flamelets*. The turbulent flame itself is treated as an ensemble of laminar Flamelets that are embedded into the flow field. The main advantage of the Flamelet model is that even though detailed information of

molecular transport processes and elementary kinetic reactions is included, the numerical resolution of small length and time scales is not necessary. This avoids the well-known problems of solving highly nonlinear kinetics in fluctuating flow fields and makes the method very robust. Only two scalar equations have to be solved independent of the number of chemical species involved in the simulation. Information of laminar model flames are pre-calculated and stored in a library to reduce computational time. On the other hand, the model is still restricted by assumptions like fast chemistry or the neglecting of different Lewis numbers of the chemical species.

The following list outlines the assumptions made to derive the Flamelet model:

- Fast Chemistry
- Unity Lewis numbers for all species, (Le =1)
- Combustion is in the Flamelet Regime
- Two feed system, i.e., fluid composition at boundaries must be pure "fuel," pure "oxidizer" or a linear blend of them.

BURNING VELOCITY MODEL

In premixed and partially premixed flames, the flamelets have a discontinuity between the burnt and the un-burnt regions; therefore the model for premixed or partially premixed combustion can be split into two independent parts:

• Model for the progress of the global reaction: Burning Velocity Model (BVM), also called Turbulent Flame Closure (TFC) [26]
   • Model for the composition of the reacted and non-reacted fractions of the fluid: Laminar Flamelet with PDF

In this model a scalar (Reaction Progress) subdivides the flow field in two different areas, the burnt and the un-burnt mixture. Burnt regions are treated similar to a diffusion flame whereas the unburnt region is represented by the cold mixture. The mass fractions in the non-reacted fraction of the fluid, $Y_{i,fresh}$, are obtained by linear blending of fuel and oxidiser compositions. The species mass fractions in the burned fraction of the fluid, $Y_{i,burned}$, are computed by applying the flamelet model.